Nuclear Instruments and Methods in Physics Research A 624 (2010) 334–339

Contents lists available at ScienceDirect

Nuclear Instruments and Methods in Physics Research A

journal homepage: www.elsevier.com/locate/nima

Experimental and theoretical study of the signal electron motion in fully depleted silicon

N. Kimmel [a,d,*], R. Andritschke [a,d], R. Hartmann [b,d], P. Holl [b,d], N. Meidinger [a,d], R. Richter [c,d], L. Strüder [a,d]

[a] Max-Planck-Institut für extraterrestrische Physik, Postfach 1312, D-85741 Garching, Germany
[b] PNSensor GmbH, Römerstr. 28, D-80803 München, Germany
[c] Max-Planck-Institut für Physik, Postfach 401212, D-80712 München, Germany
[d] MPI-Halbleiterlabor, Otto-Hahn-Ring 6, D-81739 München, Germany

ARTICLE INFO

Available online 13 May 2010

Keywords:
pnCCDs
Mesh experiment
Charge collection
X-ray detectors
Electron dynamics
Electron mobility

ABSTRACT

Imaging spectrometers based on a fully depleted silicon substrate are sensitive over the whole device volume. Therefore, a high detection efficiency for X-rays of up to 20 keV is achieved. Our experimental method facilitates measurements of the detected signal pulse height in a pixel as a function of the photon conversion position in the pixel array. Further analysis of the measurements delivers the size of a signal electron cloud after its drift from the photon conversion position to the storage cells. These results can be used to reconstruct the conversion position of each detected X-ray photon. A reconstruction accuracy of 1 μm can be achieved with a pixel size of 51 μm. Complementary to the measurements, we have created a physical model of the signal electron collection process. The change of the drift mobility with the electric drift field strength in the detection volume is considered in order to correctly describe the drift speed of the charge cloud. The electric field values and the values of the charge density in the detector volume are delivered by numerical device simulations with the software package 'TeSCA'. Comparisons of the simulations with the measurements confirmed the correctness of the applied physical model. We have thus established a method which enables device designers to simulate the process of signal charge collection in future detector concepts.

1. Introduction

X-ray imaging spectrometers based on a fully depleted silicon substrate are currently used in material structure analysis experiments at synchrotron light sources as well as on X-ray astronomy satellite experiments. A new field of application for this type of X-ray detector are experiments at free electron lasers. An X-ray spectrometer based on a fully depleted silicon substrate is realized in the pnCCD, an array detector with a sensitive thickness of 450 μm and pixel sizes from 51×51 to $150 \times 150\,\mu m^2$ [1]. A pnCCD combines a spectroscopic resolution of 140 eV at 5.9 keV and a high sensitivity for X-rays up to 20 keV with an imaging capability at array sizes of currently up to 512×1024 pixels [2].

2. Physical background

Signal charge collection in a pnCCD begins with the conversion of an X-ray photon into electron–hole pairs. In the energy range from 200 eV to 10 keV, an average value of 3.65 eV is needed for the generation of one electron–hole pair. In a pnCCD based on a fully depleted silicon substrate with 450 μm thickness, X-ray photons with an energy of 10 keV or less pass through the entrance window on the back side and are absorbed inside of the fully depleted bulk where the electrical field strength is above 1000 V/cm. The initially generated electron–hole cloud comprises a spherical volume with a typical radius of 0.5 μm [4]. During the first 1.0×10^{-12} s after their generation, the electrons are separated from the holes by the drift field in the bulk.

In the case of photon energies below 6 keV as used for our experiments, the attenuation length is below 30 μm [3]. Therefore, the signal electrons drift over a distance of typically 400 μm to the storage cells in the pixel array, as shown in Fig. 1. Beginning from the moment of electron–hole separation, the charge cloud expands due to diffusion and electrostatic repulsion [5]. The expansion of the charge cloud continues until it interacts with the lateral field components created by the structures on the register side. In the moment when the charge cloud is captured by the electric potential maxima of the pixels, it has a Gaussian density distribution with a typical σ radius of 9 μm for a detector with a thickness of 450 μm, a back contact voltage of −250 V, and at a temperature of 190 K [9]. The most significant parameters of

* Corresponding author at: Max-Planck-Institut für extraterrestrische Physik, Postfach 1312, D-85741 Garching, Germany. Tel.: +49 89 83940078.
E-mail address: nik@hll.mpg.de (N. Kimmel).

0168-9002/$ - see front matter © 2010 Published by Elsevier B.V.
doi:10.1016/j.nima.2010.05.005

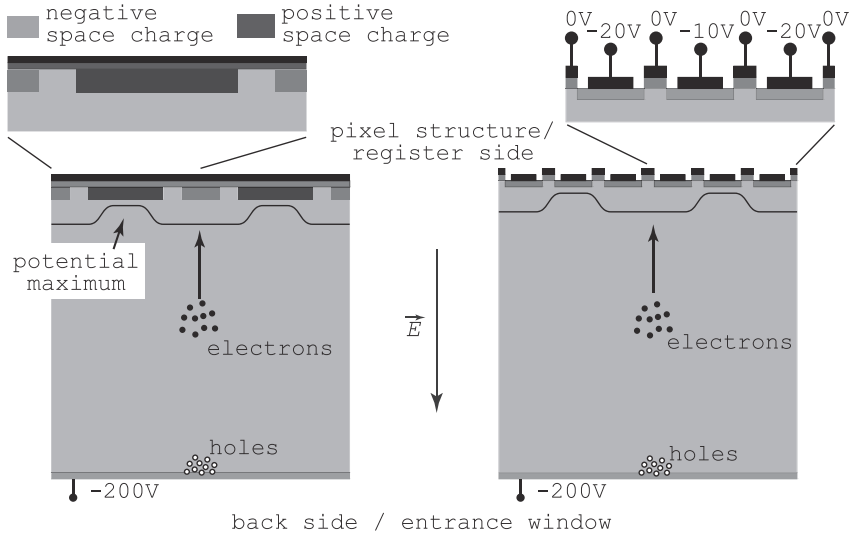

Fig. 1. Charge collection in a pnCCD. The electrons drift opposite to the field vector towards the register side. In the charge transfer direction (right-hand side), the register voltages define lateral potential maxima where the electrons are collected. In the row direction (left-hand side), the potential maxima are defined by the depleted space charges. The combination of register voltages and space charges results in a rectangular array of lateral potential maxima, the storage cells or pixels.

our model for the measured charge cloud size are the drift distance $\Delta z_{\mathrm{drift}}$, the drift field strength $\mathcal{E}_z$, the temperature T and the electron mobility $\mu_{e^-}(T,|\mathcal{E}|)$.

3. Measurement method

We have successfully adapted the method of the virtual pixel scan or 'mesh experiment' as originally proposed by Tsunemi [6,7] to pnCCDs [8,9]. The mesh experiment emulates scanning of a pixel with a narrow X-ray beam of 5 μm diameter, as shown in Fig. 2. The 'mesh' is a gold foil with a thickness of 10 μm that carries a rectangular hole grid with a pitch of 150 μm and a hole diameter of 5 μm.

The hole grid covers an area of $10\times10\,\mathrm{mm}^2$ on the detector which corresponds to 4400 scanning steps. The chosen hole distance of 150 μm is close to an integer multiple of the pixel side lengths of the studied devices: 150, 75 and 51 μm. This geometrical condition simplifies the reconstruction of the individual hole positions. Our mesh position reconstruction method [8] is based on the size and position of the dark/bright patterns for the amount of collected signal charge in a pixel as shown in Fig. 2. The method determines the exact hole pitch in relation to the pixel size and can tolerate the 2% deviation of the 150 μm hole pitch from being an integer multiple of the 51 μm pixel size. Calibrated data [10] of the detected X-ray events in a mesh measurement are used for the mesh position reconstruction which determines the position of each hole with an accuracy of 1.5 μm.

The experimental setup consists of an evacuated beam line with a length of 4 m which has an X-ray tube mounted at one end and the detector chamber at the other end as shown in Fig. 3. The mesh with its assembly is mounted directly on the cooling mask of the CCD and has a distance of 2 mm from the radiation entrance window. Photons from the X-ray tube emerge from a small region with a diameter of 1 mm which acts like a point source and creates an even intensity distribution in the plane of the detector. The mesh acts as a filter which creates small illuminated spots with the diameter of the mesh holes on the radiation entrance window of the CCD. The radiation intensity is adjusted such that single photon detection and hence spectroscopy is possible. Due to the spectroscopic capability of the detector, photons from the respective K or M fluorescence lines of the anode targets can be selected for the analysis.

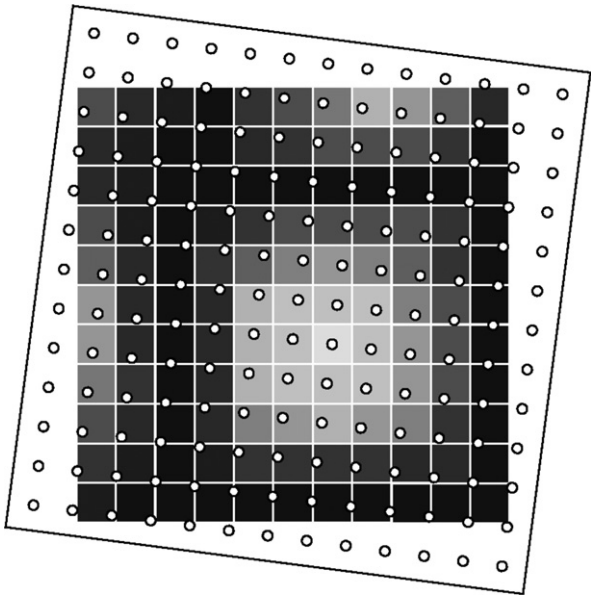

Fig. 2. Principle of the virtual pixel scan. Each hole position represents one step of a pixel scan. Given the assumption that all pixels have the same physical properties, all hole positions together represent the scanning of one 'representative' pixel. The gray shades indicate the amount of signal charge that reaches the pixel below the hole. Light shades indicate that nearly all electrons generated by a photon are collected in a single pixel, dark shades indicate that the generated electrons are distributed over more than one pixel.

3.1. Reconstruction of the charge collection function

Once the position of the mesh is determined, the X-ray event data of the pixels below each mesh hole can be rearranged into a map of the 'charge collection function' *ccf*. For each detected X-ray event, the hole position and the signal amplitudes in the surrounding pixels are recorded. This gives nine signal values in total from the (central) pixel below the hole and the eight surrounding pixels. These nine signal values are assigned to nine photon conversion positions relative to the central pixel in a map of 3×3 pixels. The ccf shows for any given conversion position the ratio of the amount of charge in the central pixel to the total amount of generated signal charge, see Fig. 4. Conveniently, the

values of the charge collection function are thus normalized to the total amount of generated signal charge. A photon which is converted in the center of a pixel thus delivers an entry in the center of the map with a value close to 1.0 and entries with values close to 0.0 in the centers of the eight surrounding pixels.

3.2. Measurement of the effective charge cloud size

The borders of the pixels in a pnCCD are effectively lateral potential barriers for electrons. In a specific depth from the pixel structure of the register side, the lateral electric field at the potential barriers causes a lateral drift movement of the signal electrons. The lateral drift vector points to the nearest local potential maximum which forms the storage cell of a pixel.

A signal electron cloud sees an increasing lateral drift field strength as it drifts from the photon conversion position to the register side. As soon as the lateral potential difference over the extension of the charge distribution in the plane of the register side is stronger than the thermal energy of a particle, electrons can no longer move freely in the charge cloud. At this point, the charge cloud begins to be separated at the pixel borders. The amount of charge that reaches a pixel is given by the integral of the projected charge density over the pixel area. We assume that the charge cloud has a Gaussian radial density profile. Then the ccf is the integral of the charge density over the area of the central pixel plotted for any given photon conversion position in a region of 3×3 pixels. In this case, the ccf is described by a combination of four error functions:

$$\mathrm{ccf}_{\mathrm{mod}}(x;y;\sigma_x;\sigma_y;x_0;x_1;y_0;y_1) = \tfrac{1}{4}\cdot(\mathrm{erf}(x;\sigma_x;x_0)-\mathrm{erf}(x;\sigma_x;x_1)) \cdot(\mathrm{erf}(y;\sigma_y;y_0)-\mathrm{erf}(y;\sigma_y;y_1)). \quad (1)$$

The values σ_x and σ_y give the size of the charge cloud in the row direction and the charge transfer direction, respectively, x_0, x_1, y_0 and y_1 are the coordinates of the pixel borders in the ccf map and the error function $\mathrm{erf}(x,\sigma,x_0)$ is defined as

$$\mathrm{erf}(x;\sigma;x_0) = \frac{2}{\sqrt{\pi}}\cdot\int_0^{(x-x_0)/(\sqrt{2}\sigma)} e^{-t^2}\,dt. \quad (2)$$

We have performed least squares fits of the ccf model given by Eq. (1) to the ccf data reconstructed from the measurements. This gives us the signal electron cloud size in the moment when it is separated and collected in the pixel structure.

Tables 1 and 2 show results of the ccf fits for two different devices, one with 75 μm pixels and 280 μm thickness, another one with 51 μm pixels and 450 μm thickness. The σ radius of the charge cloud varies between a minimum of 6 μm in the case of the 280 μm thick device and a maximum of 11 μm in the case of the 450 μm thick device. All qualitative expectations on the dependence of σ on the basic physical parameters are confirmed: Longer drift times due to either increased device thickness or lower drift field strength (lower back contact voltage V_{back}) increase σ_{row} and $\sigma_{\mathrm{transfer}}$ due to the longer time available for expansion due to diffusion and electrostatic repulsion.

The expansion of an electron cloud due to diffusion or electrostatic repulsion is described by the following expressions with the parameters T for the temperature, μ_{n} for the electron mobility, N for the number of electrons while ε is short for $\varepsilon_{\mathrm{Si}}\varepsilon_0$, the electric permittivity of silicon:

$$\sigma_{\mathrm{radius}}(t) = \sqrt{\frac{2kT}{e}\cdot\mu_{\mathrm{n}}\cdot t}; \quad r_{\max}(t) = \sqrt[3]{\frac{3\cdot Ne}{4\pi\varepsilon}\cdot\mu_{\mathrm{n}}\cdot t}. \quad (3)$$

One can see that both expressions for the charge cloud σ_{radius} or $r_{\max}(t)$ contain the term $\mu_{\mathrm{n}}\cdot t$. If t is replaced with the drift time

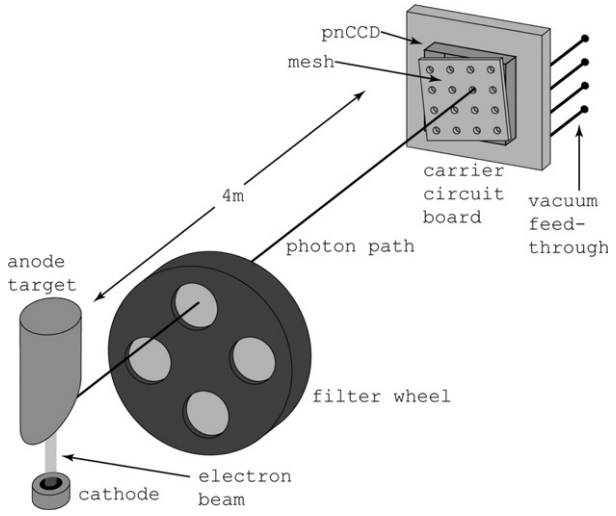

Fig. 3. Sketch of the experimental setup for mesh measurements. The X-ray tube has various anode targets including W, Ti and Cr for the W-Mα (1775 eV), Ti-Kα (4510 eV) and Cr-Kα (5415 eV) lines. The mesh is rotated by 2.5 to 4.0° with respect to the sides of the pixel array.

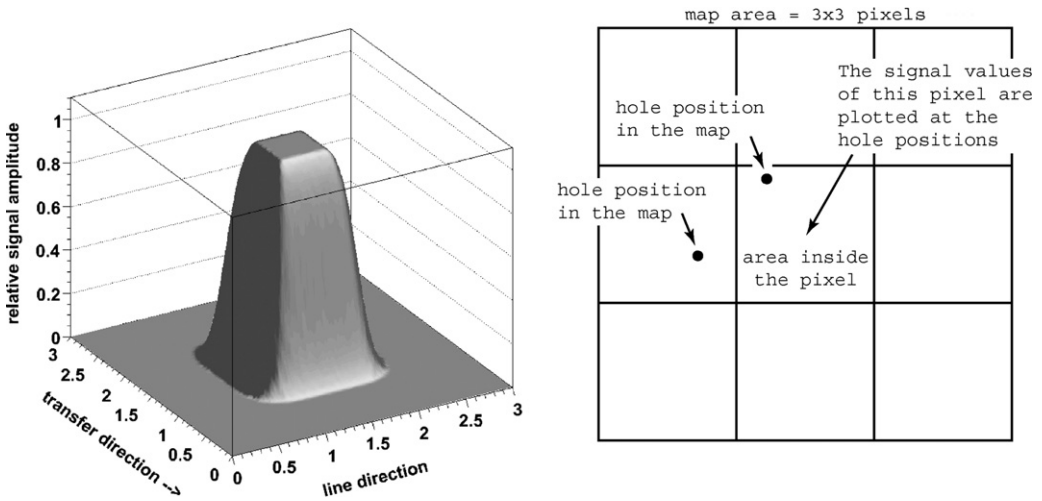

Fig. 4. Left-hand side: plot of a charge collection function (ccf) which is reconstructed from Monte Carlo simulation data of a pnCCD with 75 μm pixels. A thickness of 450 μm, a back contact voltage of −250 V, a temperature of 300 K and a photon energy of 4.5 keV were used as simulation parameters. A value of 1.0 means that all 1236 signal electrons are collected in the pixel below the photon conversion position. Right-hand side: illustration of the meaning of values in the ccf map for photon conversion positions inside and outside of the pixel where the number of signal electrons is measured.

t_{drift} of the charge cloud under the consideration that t_{drift} is inversely proportional to μ_n and an arbitrary function of the drift distance Δx, μ_n is cancelled from the expressions for σ_{radius} and $r_{max}(t)$. The remaining dependencies of the charge cloud size are the drift distance Δx, the temperature T and the electron number N:

$$\sigma_{radius}(t) = \sqrt{T} \cdot C \cdot f(\Delta x); \quad r_{max}(t) = \sqrt[3]{N} \cdot C \cdot f(\Delta x) \tag{4}$$

Table 1
Fit results of ccf data reconstructed from data sets taken with a 75 μm pixel pnCCD with 280 μm device thickness.

X-ray energy	σ_x	σ_y	Max. deviation
Temperature 193 K, $V_{back} = -90$ V ⟶			
W-Mα 1775 eV	6.96 μm	7.18 μm	+8%/−8%
Ti-Kα 4510 eV	7.54 μm	7.83 μm	+8%/−6%
Temperature 193 K, $V_{back} = -140$ V ⟶			
W-Mα 1775 eV	6.11 μm	6.66 μm	+15%/−10%
Ti-Kα 4510 eV	6.58 μm	7.19 μm	+10%/−10%
Temperature 153 K, $V_{back} = -90$ V ⟶			
W-Mα 1775 eV	6.77 μm	6.90 μm	+10%/−10%
Ti-Kα 4510 eV	7.36 μm	7.48 μm	+8%/−8%
Temperature 153 K, $V_{back} = -140$ V ⟶			
W-Mα 1775 eV	5.96 μm	6.32 μm	+10%/−10%
Ti-Kα 4510 eV	6.45 μm	6.86 μm	+10%/−10%

The x direction corresponds to the row direction in the CCD, the y direction corresponds to the transfer channel direction.

Table 2
Fit results of ccf data reconstructed from data sets taken with a 51 μm pixel pnCCD with 450 μm device thickness.

X-ray energy	σ_x	σ_y	Max. deviation
Temperature 180 K, $V_{back} = -250$ V ⟶			
W-Mα 1775 eV	8.80 μm	8.53μm	+10%/−10%
Ti-Kα 4510 eV	9.24 μm	9.03μm	+10%/−10%
Cr-Kα 5415 eV	9.27 μm	9.05μm	+10%/−10%
Temperature 180 K, $V_{back} = -180$ V ⟶			
W-Mα 1775 eV	10.21 μm	9.59μm	+10%/−10%
Ti-Kα 4510 eV	10.70 μm	10.10μm	+10%/−10%
Cr-Kα 5415 eV	10.71 μm	10.21μm	+10%/−10%

where C is a constant. The relations (4) hold true if the electron mobility is a scalar, i.e. independent of the direction in the crystal. The expected net effect is a smaller measured charge cloud size for lower temperatures if diffusion plays a dominant role in the charge cloud expansion. This effect is qualitatively confirmed by the results shown in Table 1.

The absolute deviations between the best fit models and the data are of the order of 10% and mainly due to irregularities of the used gold mesh. Generally, the ccf model of Eq. (1) which is based on the assumption of a Gaussian charge cloud form describes the measured and reconstructed ccf data correctly.

4. Numerical simulations of signal charge drift and collection

One motivation for this work is the need for a model of the signal electron motion which can be applied in the design phase of future devices. We have therefore created device simulations of

Table 3
Overview of the simulation results for the studied 75 μm pixel pnCCD.

Data type	X-ray line (eV)	T (K)	σ_x (μm)	σ_y (μm)	$\Delta\sigma_x$	$\Delta\sigma_y$
Measurement	W-Mα/1775	193	6.96	6.71	–/–	–/–
Simulation	W-Mα/1775	193	7.36	7.21	5.7%	7.5%
Measurement	W-Mα/1775	193	6.80	6.69	–/–	–/–
Simulation	W-Mα/1775	193	7.36	7.21	8.2%	7.8%
Measurement	W-Mα/1775	153	6.85	6.54	–/–	–/–
Simulation	W-Mα/1775	153	7.23	7.06	5.5%	8.0%
Measurement	Ti-Kα/4510	193	7.48	7.29	–/–	–/–
Simulation	Ti-Kα/4510	193	8.19	8.07	9.5%	10.7%
Measurement	Ti-Kα/4510	193	7.41	7.17	–/–	–/–
Simulation	Ti-Kα/4510	193	8.19	8.07	10.5%	12.6%
Measurement	Ti-Kα/4510	153	7.42	7.08	–/–	–/–
Simulation	Ti-Kα/4510	153	7.94	7.76	7.0%	9.6%
Measurement	Cr-Kα/5415	193	7.59	7.64	–/–	–/–
Simulation	Cr-Kα/5415	193	8.21	8.06	8.2%	5.5%

Each simulation is shown with the associated measurement in the row above and the errors of the resulting σ values of the charge collection function. Note that only in three cases the error of σ_{line} or $\sigma_{chn.}$ is above 10%. The measurements at 193 K for W-Mα and Ti-Kα were done twice in order to check the accuracy of the σ determination from the reconstructed ccf data.

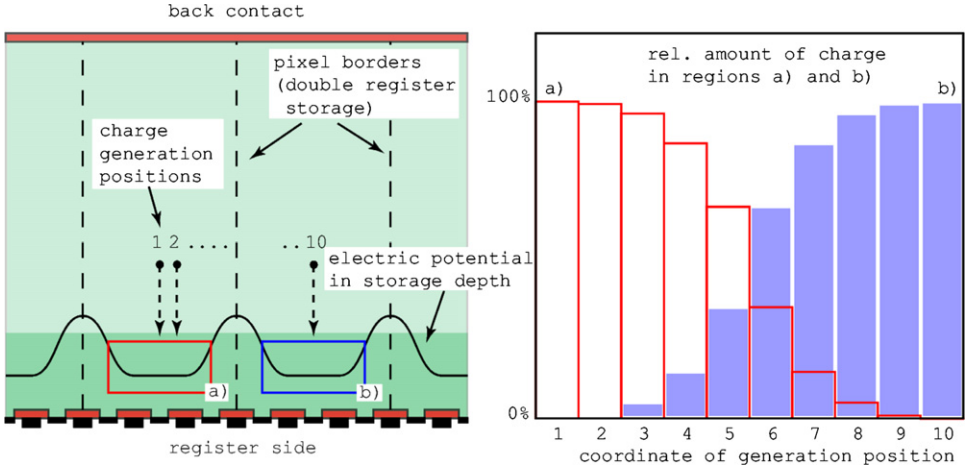

Fig. 5. Illustration of the set of device simulations that are used to simulate the charge collection function. Here, a simulation in the charge transfer direction is shown for the case of storage below two registers. Equidistant generation positions of a signal electron cloud are denoted with their index from 1 to 10. On the right-hand side, a graph shows the relative amount of charge in region (a) and (b) plotted over the charge generation positions on the x-axis.

the electric potential and the motion of the signal electrons in this potential with the software 'TeSCA'. For the metal contacts of the registers, Dirichlet boundary conditions were applied, for the MOS-gates we have used natural boundary conditions. Since we have simulated regions with a width of three pixels corresponding to nine registers, the structure of the simulation region including the register voltages could be kept symmetric to the middle axis in the z-direction, where the z-coordinate corresponds to the depth in the device. Compare Fig. 5 where the vertical axis corresponds to the z axis. Using Neumann boundary conditions at the left- and right-hand borders of the simulation region, the periodic potential structure could be correctly simulated.

Table 4
Overview of the simulation results for the studied 51 μm pixel pnCCD.

Data type	X-ray line (eV)	T (K)	σ_x (μm)	σ_y (μm)	$\Delta\sigma_x$	$\Delta\sigma_y$
Measurement	W-Mα/1775	180	9.13	8.57	–/–	–/–
Simulation	W-Mα/1775	180	8.85	9.26	−3.2%	8.1%
Measurement	W-Mα/1775	180	8.95	8.68	–/–	–/–
Simulation	W-Mα/1775	180	8.85	8.77	−1.1%	1.0%
Measurement	W-Mα/1775	180	10.48	9.78	–/–	–/–
Simulation	W-Mα/1775	180	9.16	9.55	−12.6%	−2.4%
Measurement	Ti-Kα/4510	180	9.50	9.02	–/–	–/–
Simulation	Ti-Kα/4510	180	9.56	9.98	0.6%	10.6%
Measurement	Ti-Kα/4510	180	9.37	9.18	–/–	–/–
Simulation	Ti-Kα/4510	180	9.56	9.47	2.0%	3.2%
Measurement	Ti-Kα/4510	180	10.85	10.22	–/–	–/–
Simulation	Ti-Kα/4510	180	9.81	10.21	−9.6%	−0.1%
Measurement	Cr-Kα/5415	180	9.45	9.08	–/–	–/–
Simulation	Cr-Kα/5415	180	9.67	10.09	2.3%	11.1%
Measurement	Cr-Kα/5415	180	9.39	9.17	–/–	–/–
Simulation	Cr-Kα/5415	180	9.67	9.58	3.0%	4.5%
Measurement	Cr-Kα/5415	180	10.99	10.33	–/–	–/–
Simulation	Cr-Kα/5415	180	9.91	10.30	−9.8%	−0.3%

Below each row with measurement results, the results of the associated simulation are shown together with the errors of the ccf σ in line and channel direction. Different σ results from the simulations are due to charge storage under either one or two of three registers.

The simulation results were combined into graphs of the ccf as shown in Fig. 5. For each set of parameters, two sets of simulations were performed, one of a cut along the charge transfer direction, one along a cut along a pixel row, below a storage register.

By the comparison with the measurement results it was possible to verify that the simulations correctly reproduce the measured charge collection function values. Tables 3 and 4 show an overview of the simulation results compared to the associated measurements, Fig. 6 shows plots of measured and simulated ccfs. An average error of 6% was achieved for the simulated value of the charge cloud size σ_{sim}. Due to limits of the available computa tion power and software, the simulations were performed in two dimensional domains. Under these constraints, 6% is an acceptable value for the accuracy of σ_{sim}.

In the case of the detector with 450 μm thickness, we had to use a mobility model where the longitudinal (drift direction) value of the electron mobility μ_{e^-} is smaller than the value of μ_{e^-} in the lateral direction. Otherwise, the simulated charge cloud sizes were too small compared to the measurements. One possible explanation for this is the large average drift field value of 5000 V/cm. Combined with a mobility of $\mu_{e^-} = 4234\,\mathrm{cm}^2/\mathrm{V\,s}$ at $T = 180$ K this results in an electron drift velocity at the saturation value of 1.0×10^7 cm/s [11]. In the perpendicular, lateral direction the expansion of an electron cloud is not reduced. The result of this effect is a longer drift time compared to a linear relation between the drift velocity v_{drift} and the electric field $\mathcal{E}$ and hence the larger charge cloud sizes we have observed. However, we need more measurements in order to study this effect. Device simulations can then help to deliver more information for an electron mobility model where μ_{e^-} depends on the direction of electron motion relative to the field vector and/or the crystal orientation.

Further analysis of the signal electron drift over the drift simulation time interval delivered the separation depth of an electron cloud. We have studied the simulation results for the electron distribution in the charge cloud over the drift distance until the electrons reach the electric potential maxima of the pixels. The depth where the charge cloud changes from a symmetric shape to a deformed shape due to the lateral field

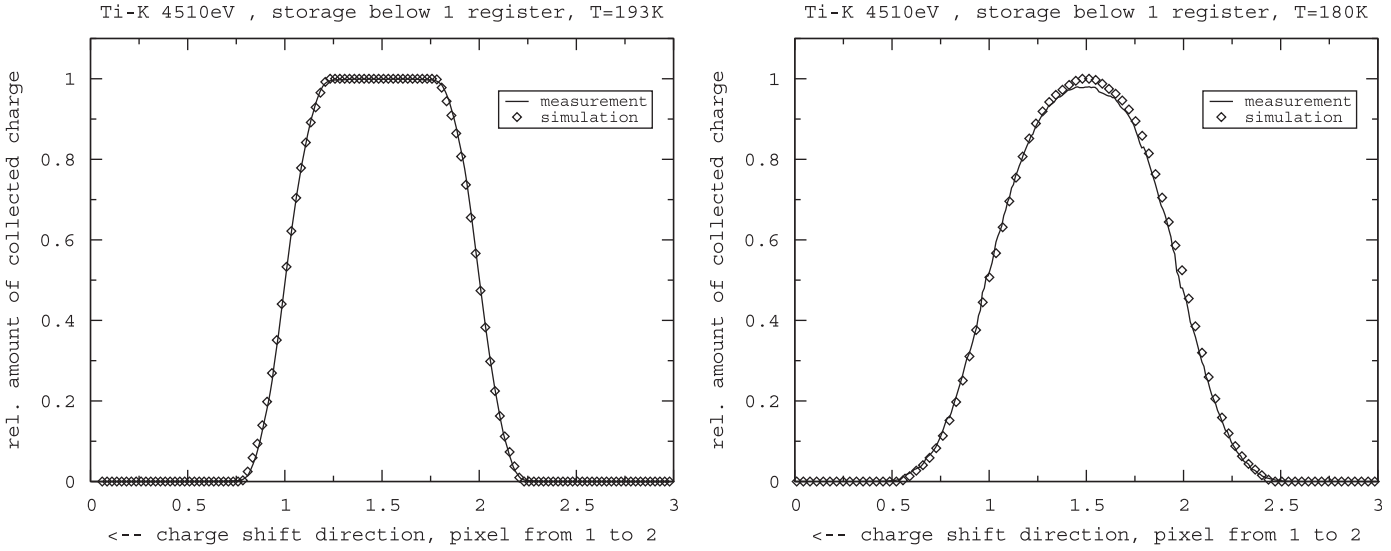

Fig. 6. Left-hand side: plot of a ccf simulation over the profile of the measured ccf for a pnCCD with a pixel size of 75 μm and a device thickness of 280 μm. Right-hand side: plot of a ccf simulation over the profile of the measured ccf for a pnCCD with a pixel size of 51 μm and a device thickness of 450 μm. In both cases, the profile plots are for the charge transfer direction and the photon energy is 4510 eV.

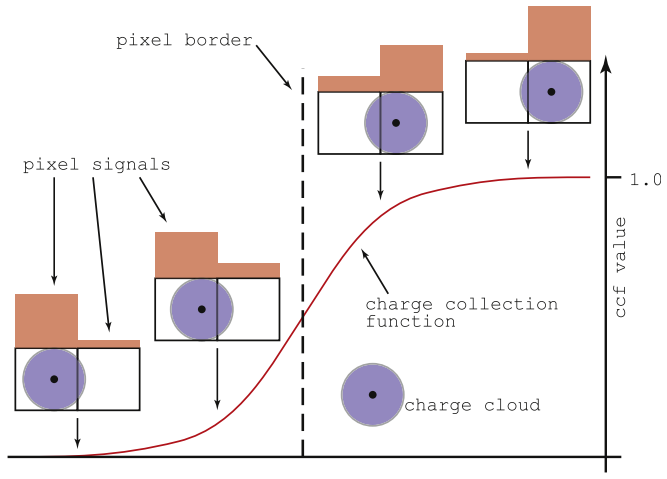

Fig. 7. Reconstruction of the conversion position for X-ray events based on known ccf values. The ratio of the pulse heights in neighboring pixels to the pulse height sum is used to determine the value of the ccf. The *x*-axis position that corresponds to the ccf value gives the photon conversion position relative to the pixel middle.

components from the register side was defined as the 'separation depth'. For pixel sizes of 75 and 51 μm, the charge cloud is separated in a depth from the register side which is equal to $\frac{1}{3}$rd of the pixel side length. The previously stated hypothesis that a signal electron cloud can expand freely until it reaches a specific separation depth close to the pixel structure was proved to be correct.

5. Application of the results: position reconstruction

If a pnCCD is operated in single photon counting mode, the pulse heights recorded in the pixels which carry the photon signal are a function of the photon conversion position. In the case of normal incidence, the conversion position is equal to the photon incidence position. The relation between the pulse heights of neighboring pixels and the photon conversion position relative to these pixels is given by the charge collection function. For a fixed set of operational parameters, the ccf depends on the photon energy. A set of ccf measurements over the required energy range is therefore needed in order to have basis for the interpolation of ccf values for an arbitrary energy in the given range.

Based on previous ccf measurements for the corresponding photon energy, the photon conversion position can be reconstructed for split events in single photon counting mode. In the case of a double event where the neighboring pixels have the same *y*-coordinate, the reconstruction works as shown in Fig. 7: The pulse height value of the right-hand pixel is divided by the pulse height sum. This ratio is located on the ccf graph and assigned to the *x*-coordinate relative to the pixel border. Finally, the obtained 'sub-pixel' coordinate is added to the *x*-coordinate of the pixel border.

In the case of a pixel size of 51 μm, a device thickness of 450 μm, a device temperature of 180 K, a back contact voltage of −250 V, a photon energy of 5 keV and a noise of two electrons ENC, nearly all converted photons deposit signal charge in more than one pixel. Position reconstruction of the resulting split events is possible with an accuracy of 0.5 μm. The statistical position uncertainty of the remaining 0.5% 'single' events in the center of the pixels is 1 μm.

6. Conclusion

The measurement method, measurements and simulation results presented here have improved our understanding of signal electron dynamics in fully depleted silicon. Although a specific device, the pnCCD, was studied in detail, the results are exemplarily for all array detectors based on fully depleted silicon substrates. The observed signal electron distribution with a Gaussian radial profile and a typical σ of 9 μm suggests a lower limit for the pixel size of single photon counting detectors. The currently realized size of 36 μm results in signal charge being spread over more than one pixel for E_{photon} from 1 to 10 keV. As a result, a position reconstruction with a resolution of 1 μm is possible with a noise/ENC of two electrons.

Furthermore, the results for high drift fields of 5000 V/cm indicate that in this case the mobility μ_{e^-} of electrons depends on the direction relative to the field vector. Since this is in contradiction to the generally assumed isotropic mobility value, we suggest further measurements for different drift field strengths in order to confirm the results presented here.

References

[1] L. Strüder, H. Bräuniger, et al., Rev. Sci. Instr. 68 (1997) 4271.
[2] N. Meidinger, et al., Proc. SPIE 6686 (2007) 66860H1.
[3] B.L. Henke, E.M. Gullikson, J.C. Davis, Atomic Data Nucl. Data Tables 54 (2) (1993) 181.
[4] H.-J. Fitting, Phys. Stat. Sol. (a) 26 (1974) 525.
[5] E. Gatti, A. Longoni, P. Rehak, M. Sampietro, Nucl. Instr. and Meth. A 253 (1987) 393.
[6] H. Tsunemi, K. Yoshita, S. Kitamoto, Jpn. J. Appl. Phys. 36 (1997) 2906.
[7] J. Hiraga, H. Tsunemi, K. Yoshita, E. Miyata, M. Ohtani, Jpn. J. Appl. Phys. 37 (1998) 4627.
[8] N. Kimmel, R. Hartmann, P. Holl, N. Meidinger, L. Strüder, Nucl. Instr. and Meth. A 568 (2006) 134.
[9] N. Kimmel, R. Hartmann, P. Holl, N. Meidinger, R. Richter, L. Strüder, Proc. SPIE 6276 (2006) 62760D.
[10] R. Andritschke, G. Hartner, R. Hartmann, N. Meidinger, L. Strüder, IEEE Nuclear Science Symposium Conference Record, 2008 (NSS '08 IEEE), 19–25 Oct. 2008, pp. 2166–2172.
[11] C. Canali, C. Jacoboni, F. Nava, G. Ottaviani, A. Alberigi-Quarata, Phys. Rev. B 12 (4) (1975) 2265.